Turbulence enhances wave attenuation of seagrass in combined wave–current flows

PNAS RESEARCH ARTICLE | ENGINEERING

Turbulence enhances wave attenuation of seagrass in combined wave–current flows

Davide Vettori[a,1], Francesco Giordana[a], and Costantino Manes[a]

Edited by Andrea Rinaldo, Ecole Polytechnique Federale de Lausanne, Lausanne, Switzerland; received July 17, 2024; accepted January 1, 2025

The wave attenuation properties of seagrasses are key to accurately predict how effective these plants are at protecting coasts from erosion and floods. While recent studies have significantly advanced the understanding of seagrass wave attenuation in pure-wave conditions, the presence of a current introduces several complications that have yet to be fully explored. In the present study, we quantify the wave attenuation of seagrass canopies in the presence of a current parallel to the direction of wave propagation via experiments conducted with dynamically scaled mimics of seagrass installed in a laboratory flume facility. The dataset we present is the largest of its kind and spans a broad range of wave properties, current velocities, water depths, and plant densities for a total of over 300 experiments. Using our experimental results, we show that the commonly employed approach of modeling wave attenuation as a result of vegetation drag works well for a range of conditions but underpredicts systematically when turbulence generated by the interaction between the seagrass canopy and the current is sufficiently strong. We then employ phenomenological arguments and experimental data to identify a nondimensional parameter that effectively quantifies the relative importance of turbulence and drag in dictating the overall observed wave attenuation. Moreover, we propose a simple but physically based modeling approach that is consistent with the proposed phenomenology and can be used for applications in coastal waters.

seagrass | wave damping | wave–current flows | turbulence

Significance

Seagrasses contribute to coastal protection through wave damping, hence representing a promising nature-based solution. Most of our knowledge stems from studies on pure-wave conditions, but in nature, it is far more common to find combinations of currents and waves. Herein, we present the largest dataset of seagrass wave damping in the presence of a current ever acquired and demonstrate that wave damping is induced by two mechanisms: drag force on seagrasses, accounted for in all previous works, and current-induced turbulence generated above the seagrass canopy, for which we provide evidence. We propose a model of seagrass wave damping that accounts for both mechanisms and can be used in models of coastal hydrodynamics.

Despite covering a negligible fraction of the ocean floor, seagrass meadows provide valuable ecosystem services (1) such as promoting biodiversity, sanitizing the water column by removing viruses and bacteria, sequestering and storing organic carbon, favoring soil accretion, stabilizing sediments, and attenuating waves for coastal protection (2–6). The recent booming interest in seagrasses is essentially driven by two factors: conservation and restoration efforts motivated by their striking global decline during the last century (7) and their use as a nature-based solution for coastal areas stemming from their potential role in climate change adaptation and mitigation (1). These two factors are strictly related as only healthy seagrass ecosystems can be expected to act as effective nature-based solutions (8, 9).

To assess the role of seagrass canopies as a nature-based solution for coastal protection, it is imperative to develop effective hydrodynamic models that quantify their ability to attenuate waves. Significant advances on this front have been achieved with models that accurately predict wave damping for monochromatic waves in the absence of currents and accounting for much of the physics of wave–plant interaction, including plant flexibility and density (10, 11). However, natural conditions along coastlines are often a combination of waves and currents, making it essential to understand the wave attenuation properties of seagrass in such conditions (12).

Much of the previous work on this topic has focused on the case of waves propagating in the same direction as the current (12–17), which can be reproduced fairly easily in laboratory settings. Results from these studies indicate that, for rigid canopies, the effect of a current on wave damping is governed by the velocity ratio $\alpha_u = U_c/U_w$ (where U_c is the current bulk velocity and U_w is the maximum longitudinal wave orbital velocity at the canopy top): For $\alpha_u \lesssim 1$, the current reduces wave damping; for $\alpha_u \gtrsim 1$, wave damping is instead enhanced (13). For seagrasses, the underlying physics is quite different because they are highly flexible plants that can reconfigure, hence reducing their effective frontal area and ultimately their form drag as compared to rigid bodies (18). Indeed, the few experimental studies performed with flexible canopies found that wave damping is reduced by a current irrespective of α_u (12, 15, 16).

Wave Attenuation Due to Drag. To ensure a relatively simple analytical tractability, as a starting point to assess the wave attenuation caused by submerged vegetation, all currently

Author affiliations: [a]Department of Environmental, Land and Infrastructure Engineering, Politecnico di Torino, Torino 10129, Italy

Author contributions: D.V. designed research; F.G. performed research; D.V. and F.G. analyzed data; D.V. and C.M. interpreted results and acquired funding; and D.V. and C.M. wrote the paper.

The authors declare no competing interest.

This article is a PNAS Direct Submission.

[1]To whom correspondence may be addressed. Email: davide.vettori@polito.it.

This article contains supporting information online at https://www.pnas.org/lookup/suppl/doi:10.1073/pnas.2414150122/-/DCSupplemental.

Published February 7, 2025.

available models use the conservation of energy for linear waves along the direction of wave propagation x (19)

$$-\epsilon_D = \frac{\partial EC_g}{\partial x} = \frac{\partial}{\partial x}\left(\frac{1}{2}\rho g {a_w}^2 C_g\right), \quad [1]$$

where ϵ_D is the rate of energy dissipation due to the drag exerted by the vegetation, E is the wave energy (per unit width of the wave front), C_g is the wave group celerity, ρ is the water density, g is the gravitational acceleration, and a_w is the wave amplitude. It is then always assumed that, regardless of whether waves are superimposed or not to a current (10–12, 16, 19), any energy lost by the waves (and consequently a reduction in their amplitudes) is due to the drag force waves exert on the vegetation, that is

$$-\epsilon_D = \frac{1}{T_w}\int_{t=0}^{T_w}\int_{z=0}^{l}\frac{1}{2}\rho C_d a_v |u_r| u_r u dz dt, \quad [2]$$

where T_w is the wave period, l is a reference length of the seagrass canopy, C_d is the seagrass drag coefficient, a_v is the seagrass frontal area per unit canopy volume, and u_r is the relative velocity between seagrass and the water, which can be approximated as the absolute fluid velocity u because it has been reported that $u_r \approx u$ for most of the wave period (20, 21). Thus, assuming u can be modeled using linear wave theory (hence neglecting any alterations caused by wave–current interaction), the wave attenuation along x can be expressed as (19)

$$\frac{a_w(x)}{a_w(0)} = \frac{1}{1 + K_D a_w(0) x}, \quad [3]$$

where $a_w(0)$ is the undisturbed wave amplitude (the longitudinal axis x has its origin at the edge of the seagrass canopy and is positive along the direction of wave propagation) and K_D is the wave attenuation coefficient of the canopy due to drag. Schaefer and Nepf (16) (hereafter indicated as SN22) developed a model to predict K_D of seagrass in the presence of a current parallel to the direction of wave propagation as

$$K_D = \frac{2}{9\pi} C_d a_v k \alpha^3 \left[\frac{9\sinh(kl_e) + \sinh(3kl_e)}{\sinh(kh)(\sinh(2kh) + 2kh)}\right], \quad [4]$$

where $C_d = \max(10KC^{-1/3}, 1.95)$ as for oscillatory flows (20), k is the wavenumber, h is the water depth, α is the ratio of in-canopy velocity to above-canopy velocity as modeled by Lowe et al. (22), and l_e is the canopy effective length, which is defined as the length required of a rigid body to experience the same drag force as the flexible body being considered (and assuming the two bodies have the same cross-section) (23). Based on the work of Lei and Nepf (10), SN22 suggests l_e can be modeled as

$$l_e/l = 0.9(Ca_{wc})^{-1/3} l_b + l_r, \quad [5]$$

where 0.9 is a numerical coefficient stemming from the best fit of wave attenuation data in pure wave conditions (10), l_b and l_r are the length of the flexible and rigid part of a seagrass (such that the total seagrass length $l = l_b + l_r$), and Ca_{wc} is the Cauchy number in combined wave–current flows (16). This formulation is consistent with the way seagrass mimics employed by SN22 in their experiments were designed, as they consisted of multiple flexible blades of length l_b held together by a rigid shoot of length l_r. The Cauchy number Ca_{wc} employed in SN22 is defined as (21)

$$Ca_{wc} = \frac{1}{2}\frac{\rho C_d b l_b^3}{EI}\left(U_{in}^2 + \frac{1}{2}{U_w}^2\right), \quad [6]$$

where b and EI are the width and flexural rigidity of the blades, and U_{in} is the mean in-canopy velocity predicted as the sum of a wave-induced mean velocity (24) and a current-induced mean velocity (25) (see the models of in-canopy flow velocity in *SI Appendix*, i.e., Eqs. **1**–**3** therein). The term in brackets quantifies the square module of a velocity related to the time-averaged drag force acting on a blade.

In addition to the use of linear wave theory, SN22 employs the following assumptions:

1. the drag force is dominant over inertial forces (i.e., the Keulegan–Carpenter number $KC = U_w T_w / b \gg 1$);
2. the Doppler effect is negligible (i.e., $C_g \gg U_c$) so that wave characteristics are not affected by the current;
3. waves account for most of the drag force on the seagrasses (i.e., $U_w > U_{in}$);
4. the wave orbital excursion at the canopy top A_w is short compared to the seagrass (i.e., $l/A_w \geq 1$), in such a way that linearized Euler–Bernoulli beam theory is valid and Eq. **5** retrieved.

Schaefer and Nepf (16) demonstrated that their model was capable to predict well the available experimental data meeting such assumptions, so we employ SN22 as the benchmark to interpret the experimental results presented herein.

Overview of the Present Work. We carried out the experiments in a 50 m long and 0.61 m wide laboratory flume with uniform canopies of dynamically scaled seagrass mimics to estimate the associated wave attenuation coefficients in the presence of currents parallel to the direction of wave propagation. The mimics were 0.1 m long with four 2 mm-wide blades and were installed so as to form a 4 m long canopy covering the whole width of the flume. We employed four canopies with a different number of mimics per square meter to vary canopy roughness density $\lambda_f = A_f/A_t$ (where A_f and A_t are the canopy frontal area and the underlying bed surface area, respectively) from 0.19 to 1, thus considering transitional (i.e., $\lambda_f \approx 0.1$) to dense (i.e., $\lambda_f \gg 0.1$) canopies (26). By altering extensively wave frequency and amplitude, current bulk velocity, and water depth, our experiments covered the following range of relevant dimensionless parameters: $Ca_{wc} = 11$ to 454; $KC = 6$ to 134; the blade Reynolds number $Re_b = U_c b/\nu = 134$ to 327, where ν is the water kinematic viscosity; $U_c/U_w = 0.3$ to 15; and the submergence ratio $h/l_d = 4$ to 14 (where l_d is the mean deflected height of the canopy—recall that the mimics are flexible), which includes shallow (i.e., $h/l_d < 5$) and deeply submerged (i.e., $h/l_d > 10$) canopy flows (26). Thus, to the best of our knowledge, the dataset presented herein represents the largest ever investigated for wave attenuation over seagrass mimics in combined wave–current flows and includes an unexplored range of both $\lambda_f < 3.1$ and $U_c/U_w > 2.5$.

During the experiments, the wave amplitude a_w was monitored along the seagrass canopy using wave gauges so that empirical wave attenuation coefficients (hereafter indicated as K_{data}) could be estimated by fitting Eq. **3** to the measured values of $a_w(x)/a_w(0)$ along x. A Laser Doppler Anemometry (LDA) system was employed to measure the longitudinal velocity component u at a single point approximately 1cm above the maximum height of the canopy to prevent potential interference between laser beams and mimic blades. The deflection of the canopy, in response to wave and current forcing, was recorded using a camera placed at the side of the flume (see *Materials and Methods* for more details).

The aim of the paper is threefold: first, to demonstrate that wave decay is not only caused by drag forces, as assumed in SN22 and all available models from the literature (e.g., ref. 12), but can also be induced by turbulence as generated by the interaction between the current and the seagrass canopy; second, to propose a nondimensional parameter that quantifies the relative importance of turbulence over drag forces in dictating wave decay; and third, to propose an analytical model that accounts for both mechanisms to predict such a decay.

Results and Discussion

First, we compare the measured wave attenuation coefficients K_{data} with the predictions of Eq. **4**. As displayed in Fig. 1, the model significantly underestimates K_{data}, with an agreement of 0.68:1 ($R^2 = 0.70$). The potential causes of this underestimation are discussed next. Approximations in the estimation of C_d can be excluded because C_d values being used by SN22 in Eqs. **4**–**6** are those for pure wave conditions, which are always slightly higher than those for wave–current conditions (27). Therefore, we would expect this approximation to lead SN22 to a systematic overprediction of K_{data}. A careful scrutiny of our experimental data indicates that SN22 performs well for cases wherein $U_{in}/U_w < 1$ (1:1, $R^2 = 0.93$, note that SN22 was validated in such conditions), while it struggles for larger values of U_{in}/U_w with most data points below the 1:1 line (Fig. 1). Notably, such a deviation is not sensitive to the exact definition of l_e, C_g, and U_{in}, and it does not seem to be related to a poor modeling of the relative velocity between water and seagrass blades (u_r) as proposed in the literature (17, 28) (see the sensitivity analysis reported in *SI Appendix*). The results of our analyses suggest that there is an overlooked physical mechanism in play. In what follows, we demonstrate that such a mechanism is most likely dictated by wave–turbulence interaction.

On the Effect of Turbulence on Wave Decay. To explore the potential effect of turbulence on wave attenuation, we focus on LDA measurements of the longitudinal velocity component u taken just above the canopy top. In all experiments, the time series of u displays low-frequency oscillations superimposed to the otherwise dominant wave-induced motions (see example in Fig. 2*A* and additional examples in *SI Appendix*, Fig. S5). To assess the contribution of these different hydrodynamic features to the energy (i.e., variance) of longitudinal velocity fluctuations, we compute the power spectral density S_{uu} of u time series. Results indicate that the observed low-frequency oscillations correspond to large spectral estimates S_{uu} occurring at frequencies $f < 0.3$ Hz (i.e., $f \ll f_w$, see example in Fig. 2*B*; $f_w = 1/T_w$ is the wave frequency), which are compatible with the presence of energetic turbulent structures of size comparable to the canopy height or larger (up to about the flow depth), as reported for steady turbulent flows (i.e., currents) over aquatic vegetation (29). The energy ratio of such large-scale (and current-induced) turbulent structures to wave motion can be roughly estimated as $\gamma = \int_{f_m}^{f_{wm}} S_{uu}df / \int_{f_{wm}}^{f_{wM}} S_{uu}df$ (with f_m being the lowest resolved frequency, and f_{wm} and f_{wM} being defined in *SI Appendix*), where the range $f_m - f_{wm}$ bounds the spectral region associated with large turbulent structures (see the blue shaded area in Fig. 2*B*), while the range $f_{wm} - f_{wM}$ bounds the spectral peak induced by wave motion (see the red shaded area in Fig. 2*B*)—additional examples are visible in *SI Appendix*, Fig. S5. Fig. 2*C* indicates that K_D/K_{data} has a clear dependence on γ: SN22 performs well for $\gamma \lessapprox 0.1$ (i.e., $K_D/K_{data} \approx 1$), while for $\gamma \gtrapprox 0.1$ there is a systematic underestimation of K_{data}. This suggests that as long as large-scale turbulent structures are weak compared to wave motion, namely, $\gamma \ll 1$, wave dissipation is mainly driven by the work of the drag force against the mean flow as per SN22. Instead, when turbulent structures become more energetic, they contribute significantly to wave attenuation.

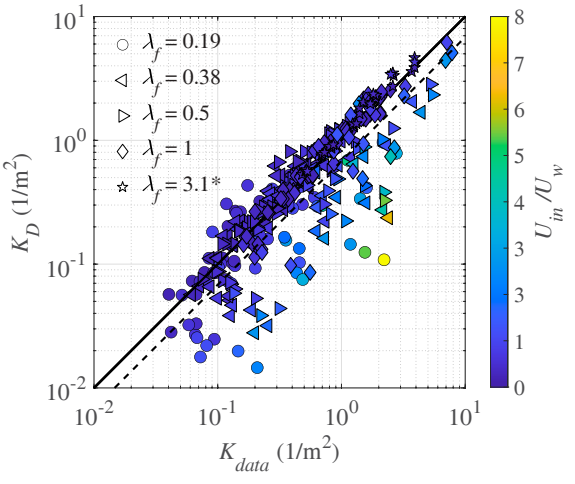

Fig. 1. Measured wave attenuation coefficient (i.e., K_{data}) versus prediction of Eq. **4** (i.e., K_D) sorted by canopy roughness density (data from Schaefer and Nepf (16) are included and highlighted with $*$ in the legend). Marker's color is scaled with the value of U_{in}/U_W (where U_{in} is the mean in-canopy velocity and U_W is the maximum wave orbital velocity at the canopy top), which ranges from 0.2 to 8 (see colorbar). The solid line denotes a 1:1 agreement, and the dashed line the best linear fit for our data ($y = 0.68x$, $R^2 = 0.70$).

Dimensional Arguments. Since γ can be estimated only from very specific and often not available velocity measurements, we now identify an equivalent diagnostic (nondimensional) parameter that can be calculated from easy-to-retrieve bulk properties of the flow. This is important since such a parameter can help to easily discern whether turbulence-induced decay needs to be accounted for (or not) when modeling wave evolution in coastal waters. We argue that in a combined wave–current flow, the relative importance of turbulence- over wave-induced fluid motion, as expressed by γ, can be represented by the parameter β defined as

$$\beta = \frac{(h - l_d)u_*}{\lambda_w U_w}, \qquad [7]$$

where u_* and $(h - l_d)$ are the friction velocity of the current (herein estimated as per Ghisalberti and Nepf (30), see *SI Appendix* for details) and a characteristic length scale associated with large-scale turbulence structures of the current (note that $h - l_d$ is the mean unvegetated water depth), respectively, and λ_w is the wavelength. Hence, β can be interpreted as the ratio of an eddy viscosity of the current (i.e., $(h - l_d)u_*$) to an equivalent parameter associated with wave motion at the canopy top (i.e., a wave eddy viscosity $\lambda_w U_w$), namely, the region around which turbulent kinetic energy and turbulence production are at their peak, thus the location that is most dynamically active over the water column (e.g., ref. 31).

We check the validity of β as the nondimensional parameter governing turbulence-induced wave decay by plotting K_D/K_{data} versus β in Fig. 3 *A*–*D*. Each panel displays a plateau region where $K_D/K_{data} \approx 1$, namely, where drag is the dominant source of wave decay, and a descending region where turbulence effects become significant. The value of β corresponding to the crossover

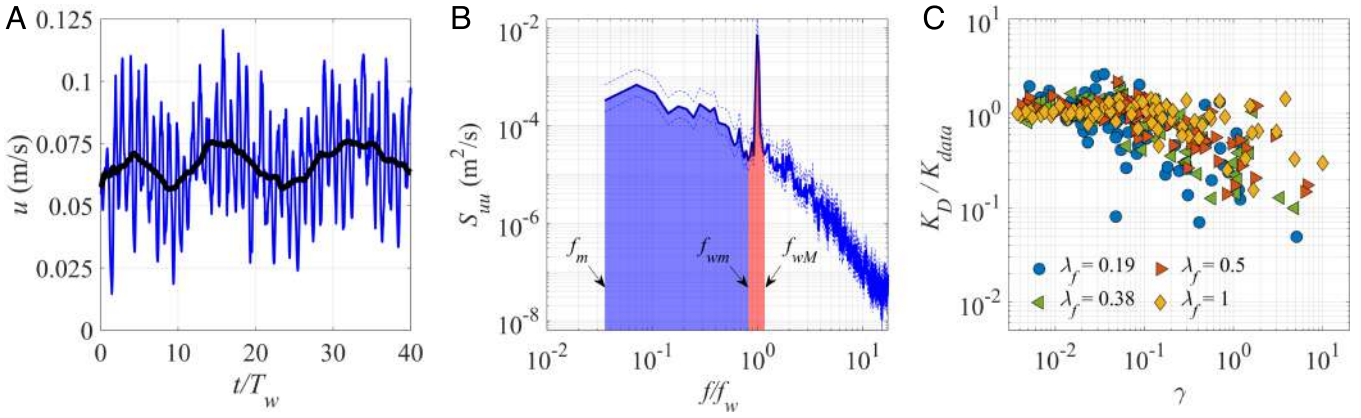

Fig. 2. (*A*) Time series of longitudinal flow velocity u above the canopy top (Test ID01 with $h = 0.2$ m, $U_c = 0.075$ m/s, 251 plants/m^2, see Table 1); the blue line denotes the raw data sampled at 25 Hz, the thick black line denotes a moving average with a width of 5 wave periods. (*B*) Power spectrum S_{uu} of the longitudinal velocity component u versus frequency components f normalized with the wave frequency f_w (Test ID01 with $h = 0.2$ m, $U_c = 0.075$ m/s, 251 plants/m^2). The dashed lines denote the 90% upper and lower CIs of S_{uu}. The blue and red shaded areas represent the energies associated with the large-scale turbulent structures and the wave motion, respectively. (*C*) Ratio of predicted (K_D) to measured (K_{data}) wave attenuation coefficient sorted by canopy roughness density as a function of the energy ratio γ defined as the ratio between blue and red shaded areas in panel (*B*).

between the two regions increases with increasing the canopy roughness density (see vertical dashed lines in Fig. 3 *A–D*, which shift from $\beta = 5 \times 10^{-3}$ for $\lambda_f = 0.19$ to $\beta = 4 \times 10^{-2}$ for $\lambda_f = 1$). This should be expected because, with increasing λ_f, the frontal area exposed to the flow and thus the drag forces exerted by the seagrass models become larger, meaning that a (relatively) higher turbulence level (i.e., higher β) is required to make a detectable effect on wave attenuation. Clearly, λ_f-effects are not entirely captured by β as this is not effective in describing K_D/K_{data} for all the investigated canopies. This makes sense because in Eq. 7 such effects are accounted for only in the definition of the current eddy-viscosity (which depends on λ_f through u_*), while the wave eddy-viscosity is left independent of λ_f and this is clearly nonphysical. To fix this shortcoming, we propose to scale β with the canopy roughness density, namely

$$\beta_\lambda = \frac{\beta}{\lambda_f} = \frac{(h - l_d)u_*}{\lambda_w U_w}\frac{1}{\lambda_f}. \qquad [8]$$

Thus, all our experimental data collapse nicely independently of λ_f as shown in Fig. 3*E*, highlighting the presence of two distinct regions previously identified for $K_D/K_{data} = f(\beta)$. The cross-over between the drag-dominated region and the region where turbulence is non-negligible lies at $\beta_\lambda \approx 3 \times 10^{-2}$. Note that Fig. 3*E* includes also data from Schaefer and Nepf (16): They are all characterized by $\beta_\lambda \approx 10^{-3}$ and, in agreement with our picture, they fall well within the drag-dominated region. This explains why turbulence contribution to wave decay was not detected by these authors. Furthermore, we performed a dedicated analysis to explore the potential dependence of K_D/K_{data} on other, more conventional, nondimensional

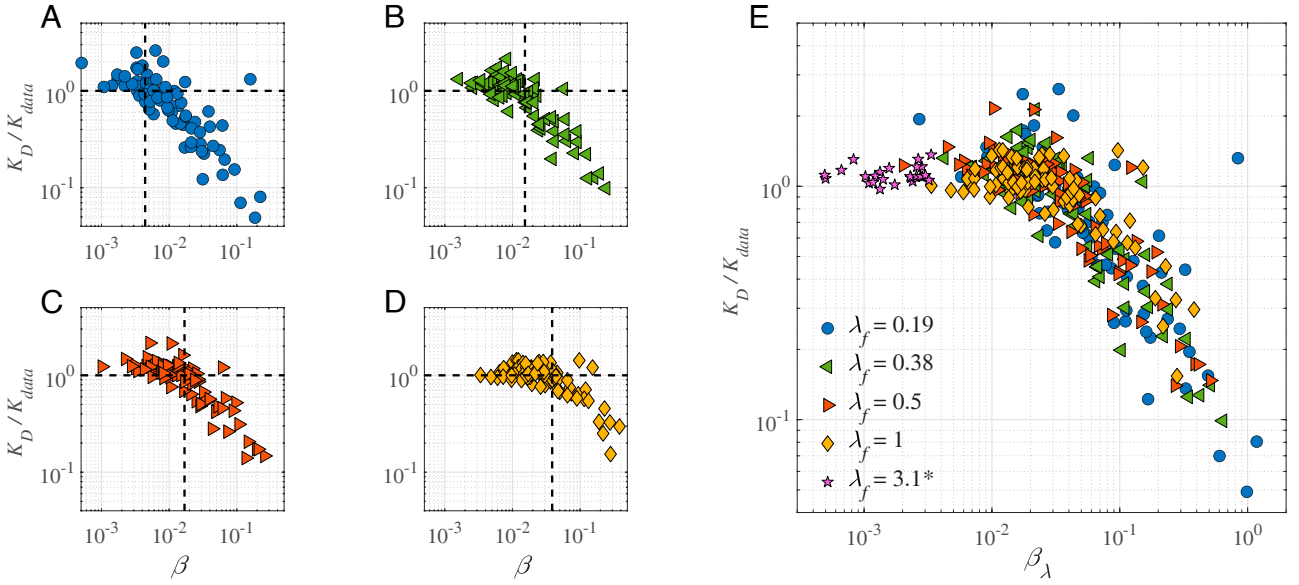

Fig. 3. (*A–D*) Ratio of predicted (K_D) to measured (K_{data}) wave attenuation coefficient for increasing roughness density (i.e., $\lambda_f = 0.19$, 0.38, and 0.5, 1) as a function of β; the horizontal dashed lines denote a perfect match between K_D and K_{data}, the vertical dashed lines denote the cross-over between the plateau region with $K_D/K_{data} \approx 1$ and the region where K_D/K_{data} decreases with β. (*E*) Ratio of predicted to measured wave attenuation coefficient as a function of β_λ (data from Schaefer and Nepf (16) are included and highlighted with $*$ in the legend).

parameters (e.g., h/l_d, U_{in}/U_w) (*SI Appendix*, Fig. S6). The results of such analysis confirm that β_λ leads to a much better data collapse than any other parameters considered. To wave decay was because β_λ was too low.

On the Universality of β. While β is not effective to appropriately account for roughness density effects on K_D/K_{data}, it can be used to address cases where turbulence is not generated by the interaction between a current and roughness elements (i.e., smooth beds whereby $\lambda_f = 0$). Such cases are discussed in this section, whose aim is to demonstrate the general validity of the proposed phenomenological arguments to characterize turbulence-induced wave attenuation via β.

In the literature, turbulence-induced attenuation of surface waves has been investigated both theoretically [mainly for the case of deep water waves see (32, 33)] and experimentally (34–38). Experimental work has been carried out for waves propagating in facilities where turbulence was generated by shear flows (i.e., in the presence of currents as in this study), oscillating grids and other turbulence-generator devices. In all these studies there is a shared consensus about turbulence being the cause of the observed wave attenuation. However, no consensus has been reached on the nondimensional parameter governing the observed attenuation rates. A very good review on the past literature on the subject and some insightful results on this matter are provided by Gutiérrez and Aumaître (39). These authors performed experiments in a little basin (0.5 m × 0.4 m) where gravity waves were generated at the interface between a shallow layer of Galinstan (a liquid alloy) and an overlying deeper layer of water. Turbulence (primarily displaying bed-normal vorticity) was externally generated via electromagnetic forcing and no roughness elements were employed at the bottom of the basin. Based on results obtained from their experimental data, Gutiérrez and Aumaître argue that the effects of turbulence on wave decay are controlled by a nondimensional parameter defined as $\Gamma_0 = \frac{\lambda_w}{a_w}\frac{\tau_w}{\tau_m} = \frac{LU_0}{a_w C_g}$, where $\tau_w = L/C_g$ is defined as the time spent by the wave energy to cross a turbulent structure of size L, $\tau_m = \lambda_w/U_0$ is the time-scale associated with the turbulent mixing rate over a length λ_w, and U_0 is a characteristic velocity of turbulence. Although developed from different physical grounds, Γ_0 is similar to β. This resemblance appears evident when considering that, in our experiments, $h - l_d$ and u_* can be considered equivalent to L and U_0, respectively. Moreover, since $U_w \sim a_w\omega$ (where ω is the circular wave frequency) and the phase velocity is defined as $C_w = \lambda_w\omega$, the main difference between Γ_0 and β relates to C_g being used in place of C_w. However, since the experiments by Gutiérrez and Aumaître (39) were carried out with $C_w/C_g \approx 1$, Γ_0 and β effectively coincide. Namely, β works well to explain wave-attenuation in both our experiments and those by Gutiérrez and Aumaître (39). This supports the hypothesis of β being a robust and universal nondimensional parameter quantifying surface-wave dissipation by turbulence regardless of how this is generated (i.e., by currents flowing over a vegetated bed in the present study, and by electromagnetic forcing in ref. 39). Moreover, β seems to work well independently of the relative angle between the direction of wave propagation and turbulence vorticity. Note indeed that in turbulent flows over vegetation (as in this study) or rough beds in general, the vorticity of large-scale turbulent structures is either oriented laterally [i.e., as in dense canopies (see, e.g., ref. 26)] or longitudinally (see, e.g., ref. 40), whereas in ref. 39 it was predominantly along the vertical coordinate.

Modeling Wave Decay by Turbulence. We now introduce a modeling framework for the evolution of surface waves in the presence of submerged vegetation that accounts for the effect of turbulence and is consistent with the phenomenological arguments presented above. From a fundamental perspective, the phenomenon of turbulence-induced wave attenuation is extremely complex to describe and model. In the case of deep water waves, Teixeira and Belcher (33) argue that wave attenuation must involve a transfer of kinetic energy from the mean (i.e., phase averaged) wave motion to turbulence, via a turbulent kinetic energy (TKE) production mechanism related to the work of turbulent stress against the mean strain rate. To the best of our knowledge, however, such a transfer mechanism has hardly been investigated for the case of combined wave–current flows in intermediate/shallow waters, let alone in the presence of seagrass canopies. Given this knowledge gap, herein, we propose a simplified modeling approach that, despite being characterized by only one tuning parameter, is effective to describe the experimental data available.

As a starting point, we assume that most of the wave attenuation caused by turbulence occurs in response to the work of the mean wave motion against the turbulent shear stress acting at the mean deflected canopy top (i.e., $z = l_d$), the region around which turbulence and TKE-production is the most intense (e.g., ref. 31). Thus, we hypothesize that the turbulent shear stress is localized at $z = l_d$ and acts as a fictitious bed for the waves, dissipating part of their energy. As a first approximation, we ignore the details of wave–turbulence interaction and assume that the flow above the canopy is dominated by wave motion. Hence, the conservation of energy along x can be written as

$$\frac{\partial}{\partial x}\left(\frac{1}{2}\rho g {a_w}^2 C_g\right) = -(\epsilon_D + \epsilon_T), \qquad [9]$$

where ϵ_D quantifies energy dissipation by drag (Eq. **2**), and

$$\epsilon_T = \frac{1}{T_w}\int_{t=0}^{T_w} \tau_{xz} u_w dt, \qquad [10]$$

is the newly introduced term quantifying wave dissipation due to turbulence, with τ_{xz} and u_w being the turbulent shear stress and the longitudinal wave orbital velocity at the deflected canopy top, respectively. For the sake of analytical tractability, we define the shear stress using the conventional form for oscillatory flows, i.e., $\tau_{xz} = \rho f u_w|u_w|$, with f being a sort of friction factor. This is convenient because substituting Eqs. **2** and **10** into Eq. **9** and estimating u_w from linear wave theory, allows to obtain the following solution

$$\frac{a_w(x)}{a_w(0)} = \frac{1}{1 + (K_D + K_T)a_w(0)x}, \qquad [11]$$

where drag and turbulence effects appear in the convenient form of two wave attenuation coefficients K_D and K_T, respectively. While K_D has been previously reported (Eq. **4**), K_T is a contribution of the present work and is defined as

$$K_T = \frac{16}{3\pi} f k^2 \frac{\cosh^3(kl_d)}{\sinh(kh)[\sinh(2kh) + 2kh]}. \qquad [12]$$

It is worth noting that Eqs. **11** and **12** are attained solving Eq. **9** following the same mathematical steps required to solve Eq. **2** and thus obtain Eqs. **3** and **4**. In line with the hypothesis

of a strong shear stress confined to a horizontal plane at $z = l_d$, we then proceed to define f starting from modeling τ_{xz} as

$$\tau_{zx} = \rho f u_w |u_w| = \rho \nu_{SL} \left(\frac{\partial u_w}{\partial z} + \frac{\partial w_w}{\partial x} \right) \Bigg|_{z=l_d}, \qquad [13]$$

where $\nu_{SL} \propto u_* t_{ml}$ is a turbulent eddy viscosity as per Ghisalberti and Nepf (30), with u_* and t_{ml} being the friction velocity and the characteristic length of large-scale eddies associated with the current, respectively, and w_w is the bed-normal wave orbital velocity at the deflected canopy top. Using linear wave theory to model u_w and w_w, first we note that $\partial u_w/\partial z \gg \partial w_w/\partial x$, then we consider the maximum velocity within a wave cycle (e.g., ref. 41) to obtain

$$f = \frac{u_*}{U_w} (k t_{ml}) \tanh(k l_d). \qquad [14]$$

Coupling Eq. **14** with Eq. **12** leads to

$$K_T = \frac{16}{3\pi} \frac{u_*}{U_w} t_{ml} k^3 \frac{\sinh(k l_d)\cosh^2(k l_d)}{\sinh(kh)[\sinh(2kh) + 2kh]}. \qquad [15]$$

Since t_{ml} is unknown, as a first approximation, we assume it to be proportional to the unvegetated water depth, namely $t_{ml} = c_t(h - l_d)$ (42), where c_t is a numerical coefficient. We estimate c_t for our dataset by minimizing the variation around the best fit, namely by maximizing R^2, and find $c_t = 3.8$. Thus, we have obtained an analytical model of wave attenuation of seagrass that accounts for both the effect of drag force and that of the large-scale turbulence generated by a superimposed current.

Model Validation. In what follows we validate our model by comparing experimental data of wave attenuation with predictions of the model as set in Eqs. **11**–**15**. To do so, we employ the dataset collected for the present work and data from Schaefer and Nepf (16). In the calculations of β_λ and K_T, we made use of the modeling framework developed by Ghisalberti and Nepf (30) to estimate u_* (*SI Appendix*, Eq. **6**) and applied $c_t = 3.8$ to both datasets. We begin by calculating the ratio K_T/K_D:

$$\frac{K_T}{K_D} = \frac{48\pi}{C_d} \frac{kl}{\alpha^3} \frac{\sinh(k l_d)\cosh^2(k l_d)}{9\sinh(k l_e) + \sinh(3k l_e)} c_t \beta_\lambda. \qquad [16]$$

Interestingly, the parameter β_λ naturally appears in Eq. **16**, which quantifies the relative importance of turbulence- versus drag-induced wave attenuation, thus supporting our phenomenological arguments. Exploiting the fact that $K_{data}/K_D \approx K_T/K_D + 1$, in Fig. 4*A* we display that predictions of Eq. **16** (plotted as a dot-dashed line) agree very well with the experimental data (plotted as markers) of both datasets. Consistently with Fig. 3*E*, the effect of turbulence on wave attenuation is significant for $\beta_\lambda \gtrapprox 2\text{–}3 \times 10^{-2}$.

Next, we employ the complete model $K_{\text{model}} = K_D + K_T$ and compare it with K_{data} in Fig. 4*B*: the experimental data are predicted with a very good accuracy, whereby $K_{\text{model}}/K_{data} = 1.03$ ($R^2 = 0.82$). It is worth noting that for cases with $\beta_\lambda < 10^{-1}$ our model tends to slightly overestimate K_{data}, particularly for our dataset. This is a range of β_λ where wave dissipation is dominated by drag, therefore, notwithstanding the simplifications introduced here to estimate K_T, it is plausible that a good part of this overestimation lies in the modeling of K_D via SN22. For example, the values of C_D employed are those for pure-wave conditions that, as previously commented, overestimate those associated with combined wave–current flows (27). Despite these limitations, our model displays an excellent performance across all available datasets.

Model's Applicability and Implications. The model can be applied fairly easily to interpret laboratory and field data alike, as in addition to the state-of-the-art model it only requires estimates of u_* and t_{ml}. For our validation, we employed measurements of the mean velocity in proximity of the canopy top to obtain u_*. Since such information is not always available, particularly under field conditions, in *SI Appendix* we present an alternative approach to estimate u_*, and thus β_λ and K_T, based on the current bulk velocity that, instead, is usually known. We find our model to work extremely well also under such scenario ($K_{\text{model}}/K_{data} = 0.96$, $R^2 = 0.80$; with $c_t = 1.6$, see *SI Appendix*, Figs. S1 and S2), suggesting that it is reliable also when flow velocity data are limited.

For the intermediate waters used in our experiments, we consider t_{ml} to scale with the unvegetated water depth and employ a tuning coefficient c_t specific to our dataset. Under field conditions, t_{ml} may need to be associated with a different

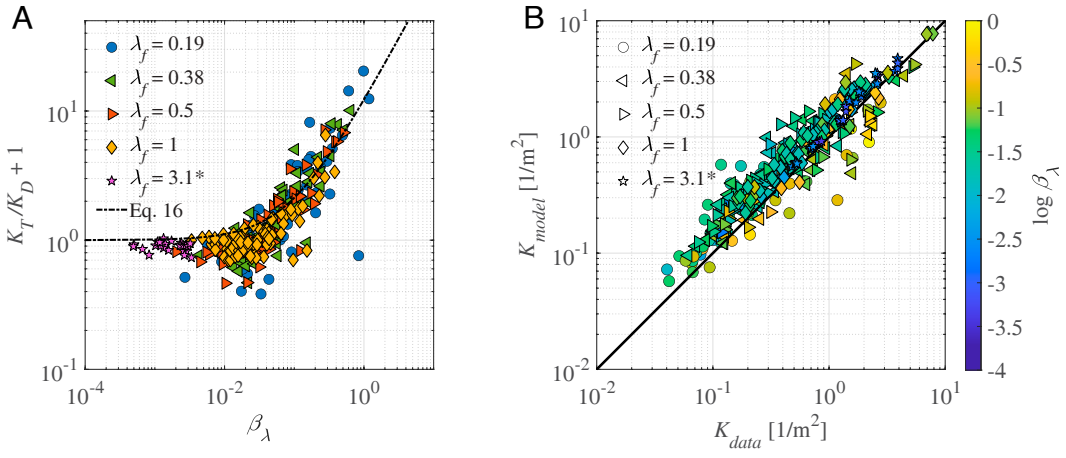

Fig. 4. (*A*) $K_T/K_D + 1$ as a function of β_λ—the dot-dashed line represents the best fit for the predictions of our data based on Eq. **16** (R^2 = 0.79). (*B*) Measured versus predicted wave attenuation coefficients ($K_{\text{model}} = K_D + K_T$, where K_D and K_T are the wave attenuation coefficients modeled with Eqs. **4** and **15**, respectively). Marker's color is scaled with the value of logβ_λ (see colorbar). The solid line denotes a 1:1 agreement, the best linear fit is $y = 1.03x$ ($R^2 = 0.82$). In both panels, data from Schaefer and Nepf (16) are included and highlighted with $*$ in the legend.

Table 1. Summary of the wave conditions tested (wave frequency f_W and amplitude a_W) sorted by water depth h

h (m)	0.2		0.3		0.4	
Test ID	f_W (Hz)	a_W (mm)	f_W (Hz)	a_W (mm)	f_W (Hz)	a_W (mm)
1	0.72	4.0	0.61	5.2	0.88	4.4
2	0.45	14.0	0.47	8.8	0.52	9.2
3	0.52	18.4	1.22	12.0	0.47	12.3
4	0.61	19.9	0.54	22.9	1.24	20.5
5	1.15	20.4	0.7	27.6	0.6	27.5
6	1.04	25.0	1.04	34.7	1.15	33.2
7	0.84	30.8	1.12	40.0	0.67	46.3
8	0.95	38.4	0.82	47.0	1.07	49.4
9	–	–	0.94	55.6	0.76	58.5
10	–	–	–	–	0.99	58.9

The values of a_W reported refer to pure wave conditions upstream of the canopy (i.e., at WG2).

length scale (and c_t may need to be tuned) to reflect a shear layer limited by factors other than the unvegetated water depth.

Our modeling framework is based on a uniform canopy with length comparable or larger than the wavelength. The effects of a mosaic of individual patches of reduced lengths are likely different and would require dedicated studies. Further, the experimental data utilized in this study are limited to the case of wave attenuation in the presence of a current parallel to the direction of wave propagation and generating turbulence with a preferential vorticity along the lateral direction. However, we demonstrated that the significance of turbulence-induced wave decay is governed by the nondimensional parameter β (also appearing in our model, see Eq. **16**), regardless of the exact orientation (i.e., the main vorticity component) of large-scale turbulent structures populating the combined wave–current flow. This is promising and suggests that the proposed modeling strategy provides a solid and general basis to address different scenarios of currents propagating at an angle with respect to waves whereby, however, we recommend further experimental and numerical studies to be carried out.

Finally, our findings indicate that seagrass canopies exposed to currents are more efficient at damping waves than previously thought, particularly at low plant densities and when deep waters are approached (Eq. **16**). This implies that seagrass ecosystems in nearshore waters may be more important for coastal protection than formerly modeled, particularly where strong currents are present and during storm surges.

Materials and Methods

Experimental Design and Setup. For the experiments, we employed seagrass mimics (see their description in *SI Appendix*, Table S1) rather than real plants because the latter are difficult to maintain healthy and with constant mechanical properties in laboratory setting (9, 43). Each seagrass mimic comprises a 10 mm long rigid dowel mimicking plant's sheath and four 100 mm long LDPE strips replicating plant's blades. The dowel covers the bottom 10 mm of the strips, resulting in a total mimic's length of 100 mm (see details in ref. 11).

The experiments were conducted in a 50 m long and 0.61 m wide open-channel flume with a smooth flat bed and equipped with a piston-type wavemaker and a submersible pump (see details in ref. 44). We installed a 4 m long canopy 19 m downstream of the wavemaker to maximize the experimental time with no wave reflections from the flume-end while ensuring fully developed hydraulic conditions. Seagrass mimics in the canopy were positioned with a staggered configuration, and four densities were employed: 251, 502, 669, and 1,338 plant/m^2. For each plant density and for the unvegetated case, 81 experiments were performed by combining three current bulk velocities U_c equal to 0.075, 0.125, and 0.175 m/s and 27 wave conditions (listed in Table 1). We ensured that a steady current (propagating along the same direction as the waves) was established by setting the incoming flow rate from the pump and the water depth by means of a sharp-crested weir located at the downstream end of the flume. On average, the current bulk velocity and the water depth at the start of the seagrass canopy were within 1% of the target value. Therefore, we can safely assume that the target value of U_c was effectively achieved in each case.

For what concerns the instrumentation, during the experiments we employed: eight resistance wave gauges (WGs) (Edinburgh Designs, Edinburgh, UK) to measure the wave amplitude along the flume/canopy, a HD camera to monitor the deflection of the canopy, and a Flow Explorer DPSS Laser Doppler Anemometer (LDA) (Dantec Dynamics A/S, Skovlunde, Denmark) to measure the longitudinal (i.e., along the direction of wave propagation) flow velocity u.

The WGs were triggered by the wavemaker, and data were sampled at 128 Hz. The first WG was mounted 2 m downstream of the wavemaker, the second WG was located 0.1 m before the upstream edge of the canopy to provide the undisturbed amplitude of the waves $a_W(0)$ used in Eqs. **3** and **11**, the remaining WGs were mounted 0.13, 0.43, 0.88, 1.57, 2.65, and 4.23 m downstream of the canopy edge, respectively (meaning that the last WG measured just beyond the downstream edge of the canopy, see Fig. 5).

The camera recorded at 100 fps and was mounted on the side of the flume so that its field of view (FOV) was centered 3.3 m downstream of the upstream canopy edge, a distance much larger than the development length for the

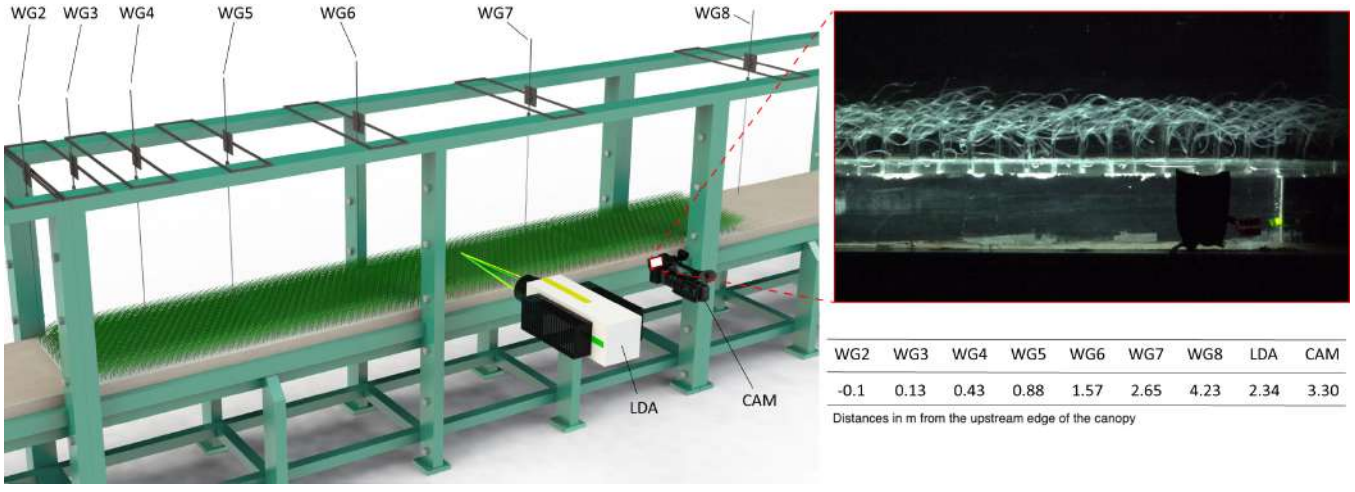

Fig. 5. Rendering of the test section of the flume covered by seagrass mimics with locations of the relevant instruments: wave gauges (WGs), Laser Doppler Anemometry system (LDA), and HD camera (CAM). In the *Inset*, a frame recorded by the camera during an experiment is shown.

in-canopy mean flow, which was equal to 1.5 m at maximum, as estimated following Chen et al. (45). To enhance the contrast between the seagrass mimics and the surroundings, a dark room was built around the test section, and a white light-sheet was employed to illuminate the mimics next to the sidewall. A small LED triggered by the wavemaker allowed for the synchronization between wave gauges and camera during data postprocessing.

The LDA was located 2.34 m from the upstream canopy edge and 80 to 90 mm above the bed depending on U_c (see dataset)–such vertical position was set to prevent potential interference of mimic blades on the LDA laser beams. The average sampling frequency was about 60 Hz, much larger than the wave frequencies employed (see Table 1).

Data Analysis. The signal from the WGs was trimmed to exclude the initial wavemaker transient and time windows when WG measurements were affected by waves reflected from the flume end. Such trimming was adjusted to cover the largest possible number of integer wave periods as estimated considering the group celerity modified by the presence of the currents (41). The same wave train was isolated for WGs 2 to 8 and the mean wave amplitude at each WG was estimated from the root mean square of the water surface displacement. The wave attenuation coefficient for each test was calculated by least square fitting Eq. **3** along x and K_{data} was obtained subtracting the wave attenuation coefficient as obtained in the same way but with an unvegetated bed at the same hydraulic conditions (see also *SI Appendix, Description of Dataset*). This allowed to isolate the effects of seagrass mimics on wave attenuation from that of the flume bed and lateral walls.

Videos were processed with MATLAB image processing tools (version R2021B) to track the deflected height of the canopy in the camera's FOV (i.e., 3.2 to 3.4 m from the upstream canopy edge). From the videos, we extracted the mean deflected height of the canopy (l_d) as the time and spatial average of the canopy height across the 0.2 m FOV. By separately analyzing the initial time period during which waves traveled from the wavemaker to the canopy and the time period wherein waves were acting on the canopy, we were able to estimate the mean deflected canopy height for both pure current ($l_{d,c}$) and combined wave–current (l_d) conditions. Note that the parameter $l_{d,c}$ is used in the estimation of mean in-canopy flow velocity as described in *SI Appendix* in detail.

Flow velocity signals collected with the LDA were postprocessed with a Dantec Dynamics Burst Spectrum Analyzer (BSA F600-2D) and dedicated software (BSA Flow Software v6.5). LDA data are notoriously sampled with an unsteady frequency (e.g., ref. 46), therefore time series were resampled at 25 Hz using a linear interpolation method to enable estimating the power spectrum of u. Since our interest lies in the low frequencies characterizing the large-scale turbulent structures, such resampling does not affect our results.

Data, Materials, and Software Availability. All post processed data collected for this work can be found in the open access repository Zenodo at the following link https://zenodo.org/records/14712025 (47). All data used for the analyses are included in the published article as part of *SI Appendix*. Raw data (e.g., time series from wave gauges, LDA, videos) are available upon request due to a large size exceeding 500 GB.

ACKNOWLEDGMENTS. We wish to thank Dr. Roberto Bosio for thorough technical support while setting up the experiments and for editing Fig. 5. D.V. thanks Mr. Elia Buono for fruitful discussions concerning the model of wave attenuation. The two anonymous reviewers are gratefully acknowledged for their constructive comments. D.V. and C.M. acknowledge funding from the European Union's Horizon 2020 research and innovation programme under the Marie Sklodowska-Curie grant agreement No. 101022685 (SHIEELD).

1. C. M. Duarte, I. J. Losada, I. E. Hendriks, I. Mazarrasa, N. Marbà, The role of coastal plant communities for climate change mitigation and adaptation. *Nat. Clim. Change* **3**, 961–968 (2013).
2. S. Temmerman *et al.*, Ecosystem-based coastal defence in the face of global change. *Nature* **504**, 79–83 (2013).
3. E. B. Barbier *et al.*, The value of estuarine and coastal ecosystem services. *Ecol. Monogr.* **81**, 169–193 (2011).
4. R. Costanza *et al.*, The value of the world's ecosystem services and natural capital. *Nature* **387**, 253–260 (1997).
5. J. T. Greiner, K. J. McGlathery, J. Gunnell, B. A. McKee, Seagrass restoration enhances "blue carbon" sequestration in coastal waters. *PLoS One* **8**, e72469 (2013).
6. J. B. Lamb *et al.*, Seagrass ecosystems reduce exposure to bacterial pathogens of humans, fishes, and invertebrates. *Science* **355**, 731–733 (2017).
7. M. Waycott *et al.*, Accelerating loss of seagrasses across the globe threatens coastal ecosystems. *Proc. Natl. Acad. Sci. U.S.A.* **106**, 12377–12381 (2009).
8. R. K. Unsworth, L. C. Cullen-Unsworth, B. L. Jones, R. J. Lilley, The planetary role of seagrass conservation. *Science* **377**, 609–613 (2022).
9. D. Vettori, S. Nieweth, J. Aberle, S. Rice, A link between plant stress and hydrodynamics? Indications from a freshwater macrophyte. *Water Resour. Res.* **57**, e2021WR029618 (2021).
10. J. Lei, H. Nepf, Wave damping by flexible vegetation: Connecting individual blade dynamics to the meadow scale. *Coast. Eng.* **147**, 138–148 (2019).
11. D. Vettori, P. Pezzutto, T. J. Bouma, A. Shahmohammadi, C. Manes, On the wave attenuation properties of seagrass meadows. *Coast. Eng.* **189**, 104472 (2024).
12. I. J. Losada, M. Maza, J. L. Lara, A new formulation for vegetation-induced damping under combined waves and currents. *Coast. Eng.* **107**, 1–13 (2016).
13. Z. Hu, T. Suzuki, T. Zitman, W. Uittewaal, M. Stive, Laboratory study on wave dissipation by vegetation in combined current-wave flow. *Coast. Eng.* **88**, 131–142 (2014).
14. C. W. Li, K. Yan, Numerical investigation of wave-current-vegetation interaction. *J. Hydraul. Eng.* **133**, 794–803 (2007).
15. M. Paul, T. J. Bouma, C. L. Amos, Wave attenuation by submerged vegetation: Combining the effect of organism traits and tidal current. *Mar. Ecol. Prog. Ser.* **444**, 31–41 (2012).
16. R. B. Schaefer, H. Nepf, Wave damping by seagrass meadows in combined wave-current conditions. *Limnol. Oceanogr.* **67**, 1554–1565 (2022).
17. R. Schaefer, H. Nepf, Movement of and drag force on slender flat plates in an array exposed to combinations of unidirectional and oscillatory flow. *J. Fluids Struct.* **124**, 104044 (2024).
18. S. Vogel, *Life in Moving Fluids: The Physical Biology of Flow* (Princeton University Press, 1994).
19. R. A. Dalrymple, J. T. Kirby, P. A. Hwang, Wave diffraction due to areas of energy dissipation. *J. Waterw. Port Coast. Ocean Eng.* **110**, 67–79 (1984).
20. M. Luhar, H. Nepf, Wave-induced dynamics of flexible blades. *J. Fluids Struct.* **61**, 20–41 (2016).
21. J. Lei, H. Nepf, Blade dynamics in combined waves and current. *J. Fluids Struct.* **87**, 137–149 (2019).
22. R. J. Lowe, J. R. Koseff, S. G. Monismith, Oscillatory flow through submerged canopies: 1. Velocity structure. *J. Geophys. Res. Oceans.* **110**, C10016 (2005).
23. M. Luhar, H. M. Nepf, Flow-induced reconfiguration of buoyant and flexible aquatic vegetation. *Limnol. Oceanogr.* **56**, 2003–2017 (2011).
24. M. Luhar, Comment on "the wave-driven current in coastal canopies" by M. Abdolahpour et al. *J. Geophys. Res. Oceans* **126**, e2019JC015644 (2021).
25. J. Lei, H. Nepf, Evolution of flow velocity from the leading edge of 2-D and 3-D submerged canopies. *J. Fluid Mech.* **916**, A36 (2021).
26. H. M. Nepf, Flow and transport in regions with aquatic vegetation. *Annu. Rev. Fluid Mech.* **44**, 123–142 (2012).
27. T. Sarpkaya, M. Storm, In-line force on a cylinder translating in oscillatory flow. *Appl. Ocean Res.* **7**, 188–196 (1985).
28. S. M. Henderson, Motion of buoyant, flexible aquatic vegetation under waves: Simple theoretical models and parameterization of wave dissipation. *Coast. Eng.* **152**, 103497 (2019).
29. M. Ghisalberti, H. M. Nepf, Mixing layers and coherent structures in vegetated aquatic flows. *J. Geophys. Res. Oceans* **107**, 1–3 (2002).
30. M. Ghisalberti, H. Nepf, The limited growth of vegetated shear layers. *Water Resour. Res.* **40**, 7 (2004).
31. R. B. Schaefer, H. M. Nepf, Flow structure in an artificial seagrass meadow in combined wave-current conditions. *Front. Mar. Sci.* **9**, 836901 (2022).
32. O. Phillips, The scattering of gravity waves by turbulence. *J. Fluid Mech.* **5**, 177–192 (1959).
33. M. Teixeira, S. Belcher, On the distortion of turbulence by a progressive surface wave. *J. Fluid Mech.* **458**, 229–267 (2002).
34. S. Kitaigorodskii, J. Lumley, Wave-turbulence interactions in the upper ocean. Part I: The energy balance of the interacting fields of surface wind waves and wind-induced three-dimensional turbulence. *J. Phys. Oceanogr.* **13**, 1977–1987 (1983).
35. H. S. Ölmez, J. H. Milgram, An experimental study of attenuation of short water waves by turbulence. *J. Fluid Mech.* **239**, 133–156 (1992).
36. J. D. Skoda, "The interaction of waves and turbulence in water," PhD thesis, University of California, Berkeley (1972).
37. T. Green, H. Medwin, J. E. Paquin, Measurements of surface wave decay due to underwater turbulence. *Nat. Phys. Sci.* **237**, 115–117 (1972).
38. J. Hoften, S. Karaki, "Interaction of waves and a turbulent current" *in Proceedings of the 15th International Conference on Coastal Engineering (ASCE, 1976)*, pp. 404–422
39. P. Gutiérrez, S. Aumaître, Surface waves propagating on a turbulent flow. *Phys. Fluids* **28**, 025107 (2016).
40. S. Cameron, V. Nikora, M. Stewart, Very-large-scale motions in rough-bed open-channel flow. *J. Fluid Mech.* **814**, 416–429 (2017).
41. R. G. Dean, R. A. Dalrymple, *Water Wave Mechanics for Engineers and Scientists* (World Scientific Publishing Company, 1991), vol. 2.
42. M. Ghisalberti, H. Nepf, The structure of the shear layer in flows over rigid and flexible canopies. *Environ. Fluid Mech.* **6**, 277–301 (2006).
43. D. Vettori, T. Marjoribanks, Temporal variability and within-plant heterogeneity in blade biomechanics regulate flow-seagrass interactions of *Zostera marina*. *Water Resour. Res.* **57**, e2020WR027747 (2021).
44. C. Peruzzi *et al.*, On the influence of collinear surface waves on turbulence in smooth-bed open-channel flows. *J. Fluid Mech.* **924**, A6 (2021).
45. Z. Chen, C. Jiang, H. Nepf, Flow adjustment at the leading edge of a submerged aquatic canopy. *Water Resour. Res.* **49**, 5537–5551 (2013).
46. C. Tropea *et al.*, *Springer Handbook of Experimental Fluid Mechanics* (Springer, 2007), vol. 1.
47. D. Vettori, Data from "Wave attenuation of seagrass in combined wave-current flows". Zenodo. https://zenodo.org/records/14712025. Deposited 21 January 2025.